Sheffield Hallam University

On the fatigue response of a bonded repaired aerospace composite using thermography

GRAMMATIKOS, Sotirios A., KORDATOS, Evangelos <http://orcid.org/0000-0002-5448-3883>, MATIKAS, Theodore E. and PAIPETIS, Alkiviadis S.

Citation:

Copyright and re-use policy

Contents lists available at ScienceDirect

Composite Structures

On the fatigue response of a bonded repaired aerospace composite using thermography

Sotirios A. Grammatikos[a], Evangelos Z. Kordatos[b], Theodore E. Matikas[c], Alkiviadis S. Paipetis[c],[*]

[a] Department of Manufacturing and Civil Engineering, Norwegian University of Science and Technology, Norway
[b] Department of Engineering and Mathematics, Sheffield Hallam University, United Kingdom
[c] Department of Materials Science Engineering, University of Ioannina, Greece

ARTICLE INFO

ABSTRACT

Lock-in thermography was employed to investigate the repair efficiency of a bonded repaired aerospace composite subjected to step-wise cycling mechanical loading. The studied component (substrate) was artificially damaged with a 5 mm circular notch and subsequently repaired with a tapered bonded patch. Critical and subcritical damage of the repaired component was monitored via thermography during 5 Hz tension–tension fatigue. The examination of the acquired thermographs enabled the identification of the patch debonding propagation as well as the quantification of the stress magnification at the patch ends and the locus of the circular notch. It was found that fatigue mechanical loading yields both thermoelastic and hysteretic phenomena with the latter being more prominent prior to the failure of the studied repaired component.

1. Introduction

Fibre reinforced polymers (FRPs) are increasingly being employed for aerospace and marine structures due to their high specific stiffness and strength [1]. FRPs have also been attractive as repair elements of aircraft, civil and naval structures as they can easily be applied to geometrically complicated configurations where repair or local stiffening is needed. Bonded repair in particular, offers distinct advantages over mechanically fastened repair systems. The application of innovative repair concepts in aircrafts requires novel non-destructive techniques which will assess the repair efficiency throughout the service life of the component and subsequently establish the process reliability for airborne structures. More importantly, enabling non-destructive technologies may also guide repair methodologies away from the widely accepted "repair and forget" principle [2].

Infrared Thermography (IrT) is a non-contact, full field non-destructive technique that can be readily applied for structural integrity assessment of structures during both in-service (lab environment) and maintenance operations. By definition, IrT operates at infrared frequencies and is sensitive to both temperature and emissivity variations [3]. IrT employs the infrared radiated energy to provide information about internal defects and discontinuities [4,5], and thus may be employed for typical inspections during maintenance. In Lock-in Thermography (LT), the thermal camera is synchronized with a periodic excitation source [6–8]. For in service applications in particular, LT is a powerful tool able to identify and follow in real time, internal damage evolution processes during cyclic mechanical loading (Fig. 1) [9,10]; in this case, the oscillating stress field can be directly acquired by monitoring the temperature variations along the surface of the loaded material [11–13]. The generated thermoelastic waves induced by the periodic stresses may act as the thermal triggering source. In the presence of stress raisers e.g. notches or cracks, induced stress gradients on the surface of the interrogated material are manifested as local temperature gradients [6,7,14].

In previous works of the authors, LT was employed to assess the patch repair efficiency on aluminium substrates [14], combined with other structural health monitoring techniques [15] as well as to rapidly estimate fatigue limit in ceramic matrix composites [16]. In this work, LT was employed to assess the bonded repair integrity on artificially damaged composite substrates when subjected to cyclic mechanical loading. The present study provides an extensive analysis and characterization of the efficiency of the bonded patch repair concept by analysing modulated thermographs of the thermoelastic signals acquired during cyclic mechanical loading as a parameter of fatigue damage. Through LT, the temperature signal is analysed in the time domain through Fourier analysis so that nonlinear signal contents (e.g. amplitude and phase of stress signal at mechanical frequency) in the evolution of temperature due to thermomechanical coupling phenomena are recorded. In this way, LT becomes independent of local optical imbalances, surface anisotropy and ambient thermal noises. The
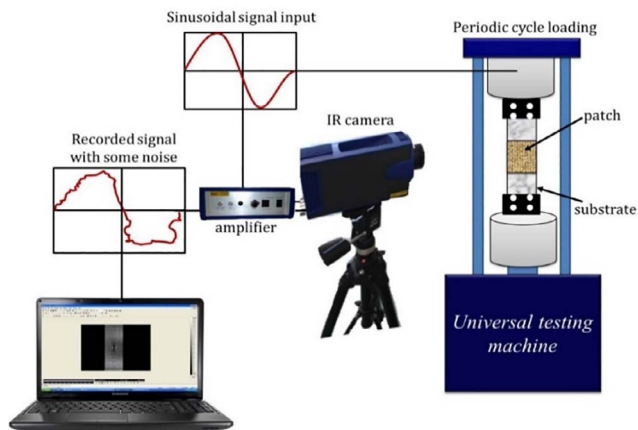
Fig. 1. Principle of on-line lock-in thermography.

employed technique can be regarded as a useful tool for bonded repair certification prior to on-site applications. Within the framework of this study, reversible thermoelastic [17] and hysteretic phenomena which accumulate to cause catastrophic failure [18,19] are analysed and discussed in relation to the thermal dynamic response of the interrogated repaired substrate. Carbon Fibre Reinforced Polymer (CFRP) laminates with central circular notches were single-side patched and subsequently subjected to cyclic mechanical loading testing. Single-side repair was chosen to simulate real practice, when access to component's sides is limited. To define the stress level where debonding initiated and propagated in a stable manner, all substrates were tension-tension fatigued starting from very low stress levels (i.e. 20% of the ultimate tensile stress of the repaired structure (σ_{uts})). The induced stress level was increased until debonding initiated at the interface between the patch and the substrate. The level of load and the corresponding number of fatigue cycles where debonding initiates, is directly relevant to the bonding efficiency of the applied patch repair. Tapered patches were studied with a view to minimising stress concentrations at the edges of the patch [20]; typical practice in bonded repairs [21]. IrT was both successful in (i) monitoring the critical failure of the patch i.e. the initiation and propagation of the debonding process and (ii) identifying the subcritical damage i.e. the stress concentrations at the locus of the patched notch and its evolution.

2. Thermal response due to dynamic mechanical loading

2.1. Thermomechanical coupling

Thermomechanical coupling (Fig. 1) has been widely employed in the past in various modes to characterize and analyse the response of materials during cyclic mechanical loading. Thermomechanical coupling by LT or the so called Thermoelastic Stress Analysis (TSA) [3,8,15,16,22–25], has been used to construct stress maps for both composite and metal materials under cyclic mechanical loading. Stress maps allow for the determination of the location of damage initiation and its subsequent evolution. The basic requirements are: (i) a periodical loading (ensuring adiabatic and linear elastic conditions), (ii) a thermal sensitive camera and (iii) a surface of uniform emissivity (i.e. finishing with a fine black matt paint) [26,27].

As early as in 1852, Lord Kelvin demonstrated the dynamical form of heat as an effect of mechanical work or else the effects of mechanical degradation on the intrinsic temperature of elastic materials [17]. Reifsnider and Williams in 1974 [28] used thermography to monitor stress induced damage in composites while in 1975 [29] Charles et al. employed TSA in artificially notched samples. In 1988, Stanley and Chan in [30] performed the TSA method to assess damage in composite materials. Bakis and Reifsnider [31] examined the relation between

strength, stiffness and remaining fatigue life to damage in composites. Other studies assessing thermomechanical mechanisms in dynamically tested composites have also been reported by Wong [32], Cunningham et al. [33] and Refs. [34–36]. Myriounis et al. [9] examined the fracture mechanics of metal-matrix composites through the monitoring of 'intrinsic energy' dissipated by thermomechanical coupling during fatigue mechanical loading [37]. The same thermographic system was employed by Kordatos et al. [24] to study the thermomechanical coupling induced in metal matrix composites during dynamic mechanical loading. In this work, thermomechanical coupling was compared with simultaneously recorded acoustic emission signals. In a later study of the team, Grammatikos et al. [15], the thermomechanical coupling observed in bonded repaired composites was studied in comparison with both acoustic emission signals and electrical measurements. More recently, the same principle was used in combination with Lamb waves technique, to study the bonded repair integrity of a patch repaired real helicopter wing by AgustaWestland (SW-4) [25].

According to the thermoelastic principle, a material subjected to cyclic mechanical loading (provided adiabatic conditions) exhibits a small reversible change in the mean temperature which is linearly proportional to the applied stress and independent of loading frequency. Adiabatic conditions are generally achieved during cycling mechanical loading. The ratio of the temperature change (the degree of which may result to partial dissipation) increases when the material is tested at significantly high stress levels. However, cyclic mechanical loading induces both thermoelastic and thermoplastic effects on the tested component. Thermoelastic phenomena are solely present when the material is stressed in the elastic region whist thermoplastic phenomena [18] are cumulatively added to the thermomechanical coupling beyond the elastic region, after irreversible processes take place [36]. In the case of cyclic loading, thermoelastic phenomena are expected to affect the material's mean temperature during testing reflecting the thermo-sensitivity of the material or the coupling between the material's mechanical and thermal states. On the contrary, prolonged fatigue loading causes thermoplastic (hysteretic behaviour) irreversible effects and subsequent extensive mean temperature increase which reflects the degradation (i.e. accumulated damage) or the irreversible transformation of the material. Intrinsic heat dissipation in polymer composites is mainly a result of the viscoelastic nature of the material, internal friction, matrix cracking, interface failure, etc. [38]. In the case of brittle fibrous composites, this monotonic temperature increase can also be attributed to heat release due to the accumulating flaws in the structure which in the presence of irreversible processes may overcome the thermoelastic effect [39]. In the case of cyclic loading, the phenomenon of intense heat generation that precedes catastrophic failure is usually recorded at the final cycles of the fatigue life of the material. Considering the above, the following observations may be made:

1. The thermoelastically induced temperature rise is only dependent on the stress state of the material and can be a direct measure of stress either globally or locally.
2. Above the fatigue limit and for adiabatic conditions, fatigue damage should always lead to a temperature monotonic increase directly related to the damage increase rate. If damage is assumed to follow a typical fatigue life diagram (see Fig. 2, [40]), then three stages should be observed, i.e. a steep temperature increase in stage (i) followed by a mild temperature increase in stage (ii) and finally a rapid temperature increase leading to failure for stage (iii) [38,41].
3. Above the fatigue limit and for non-adiabatic conditions as is typical in ambient testing, heat dissipation is counteracting with the heat induced by irreversible damage processes.

In this regime, three distinct stages can be assumed:

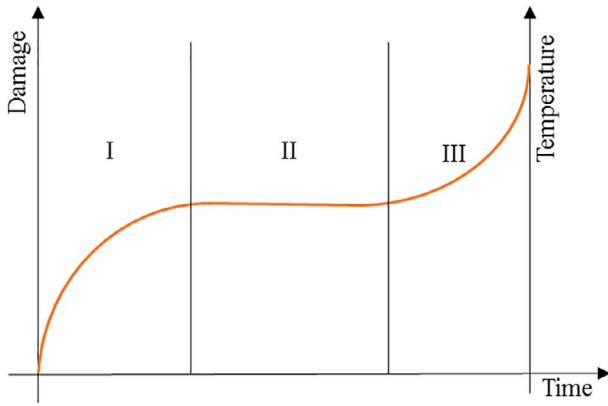a. The rate of heat distribution/dissipation H′ to the surrounding

Fig. 2. Expected damage and temperature trend during cyclic mechanical loading.

environment is higher or equal than the rate of heat produced by irreversible phenomena. In this case, the temperature of the material is reaching a steady state (no heat release) only dependent on the mean stress amplitude and again the temperature variation either globally or locally is only due to thermoelastic coupling and not to irreversible hysteretic phenomena.

b. The rate of heat distribution/dissipation is lower than the rate of heat produced by irreversible/hysteretic phenomena (not enough time for generated heat to escape). In this case there is a temperature rise (heat release) on the material. As heat distribution rate is a function of temperature, the temperature will rise and may reach a steady state at the temperature where heat distribution rate equals the hysteretically induced heat rate. Such a behaviour should be typical of stage II fatigue (Fig. 2).

c. If the damage rate is high, as in stage III of Fig. 2, temperature will rise monotonically until failure and in this case no steady state is observed.

From the above, it can be concluded that thermoelastic stress analysis is very accurate below the fatigue limit, and in the absence of hysteresis. In such the case, absolute temperature may be correlated to stress measurements if the thermoelastic coefficient of the material is known. In the case of stress raisers in the material such as in the presence of circular notches, a stress gradient is created on the specimen surface (Fig. 3). The stress concentration can be defined as $\sigma_{local}/\sigma_\propto$ where σ_{local} is the local stress concentration and $\sigma_\propto$ the stress at a distance from the notch.

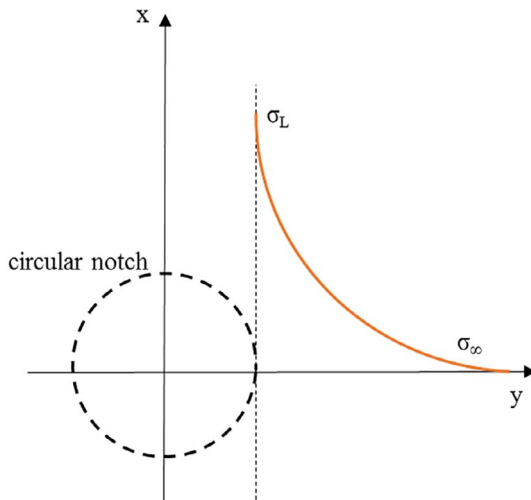According to the preceding analysis, during fatigue testing, a steady

Fig. 3. Expected generated stress gradient at the locus of the stress raiser (circular notch).

temperature state may be achieved only if (i) there is no hysteresis and (ii) damage reaches a quasi-steady state in non-adiabatic conditions, where heat distribution rate is less or equals the heat (released) rate due to hysteresis. Assuming that the local temperature variations are small in comparison to the global temperature (i.e. the heat distribution rate is practically constant along the surface) (i) the global absolute temperature variations are small and (ii) a quasi-steady stress temperature state is retained i.e. for a large enough number of cycles, the local stress concentration $\sigma_{local}/\sigma_\propto$ can be regarded as corresponding to the induced local temperature variation $T_{local}/T_\propto$.

2.2. Thermomechanical behaviour of composites

Thermal waves are generated via thermomechanical coupling and detected by a synchronized thermographic system. Assuming adiabatic elastic conditions for a thermally isotropic solid [9,10], a way to describe heat diffusion may at its simplest version be as (Eq. (1)):

$$\rho C_p \Delta T = S_{the} + d_1 \tag{1}$$

where ρ is the mass density, C_p the specific heat and constant pressure, ΔT the change in temperature in Kelvin degrees, S_{the} the thermoelastic source and d_1 the intrinsic dissipation source. The thermoelastic energy S_{the} can be described as:

$$S_{the} = -aT_0\sigma \tag{2}$$

where α the Coefficient of Thermal Expansion (CTE), T the absolute temperature and σ the sum of principal stresses. Therefore, Eq. (1) can be written as:

$$\Delta T = \left(-\frac{\alpha}{\rho C_p}\right) T_0 \Delta\sigma + d_1, \tag{3}$$

or

$$\Delta T = K_m T_0 \Delta\sigma + d_1 \tag{4}$$

where K_m the thermoelastic coefficient and $\Delta\sigma$ represents the change in the sum of principal stresses. Carbon fibres are thermally anisotropic, as they possess a negative CTE in the longitudinal direction and a positive CTE in the transverse direction [42–44]. However, Wong reported positive CTE values at the two principal directions [32]. In all cases, the thermoelastic response of the material is different in the two principal directions and is more accurately described for plane stress conditions and an orthotropic solid by the following expression and by assuming solely thermoelastic effects (Eq. (5)):

$$\Delta T = K_{mL} T_0 \Delta\sigma_L + K_{mT} T_0 \Delta\sigma_T + d_1 \tag{5}$$

where the subscripts L and T denote the longitudinal and transverse directions respectively [19,22,45]. What is typically shown by Eq. (5) is that the thermoelastic response of a loaded material is the sum of the thermoelastic response of the stresses in the two principal directions which cannot be distinguished.

In the case of low stress levels, the intrinsically dissipated energy due to irreversible hysteretic phenomena is negligible compared to the thermoelastic energy source. Therefore, Eq. (5) can be rewritten as:

$$\Delta T = K_{mL} T_0 \Delta\sigma_L + K_{mT} T_0 \Delta\sigma_T \tag{6}$$

Hence, depending on the sum of the terms in Eq. (6), the temperature of a thermally anisotropic material may increase or decrease during tension and vice versa during compression [11,13]. Another issue that is frequently raised relates to the imprint of the through thickness anisotropy to the surface temperature, which is of particular importance for a laminated structure. Melvin et al. [39], concluded that the surface temperature differences are attributed to the whole laminate and not only to the top lamina of the examined multi-layered composite. In this case the thermal anisotropy as described in Eq. (2) should be accounted for, even for orthotropic or transversely isotropic symmetries. Wong et al. [46] reports that the thermal properties of each

lamina affect significantly the surface thermographic measurements and the material cannot be examined as homogenous and isotropic. Dunn et al. [47] stated, a quasi-isotropic laminate such as a 0°/90° is seen by the thermographic system as an isotropic material. At the same paper it is argued that the 5 Hz cyclic loading frequency is in the frequency limits accounted for adiabatic conditions in thermoelastic stress analysis. In other approaches, the temperature gradient is attributed to the topmost layer which may act as a "strain witness" [48]. The strain witness layer is related to the resin rich surface or even the black matt paint employed to simulate the emissivity of the black body. Worth to mention, the resin layer affects the temperature transfer from the internal to the exterior when its thickness is high enough. In addition, the thickness of the reinforcement has to be lower enough compared to the surface resin layer in order the latter to act as strain witness.

In the case of orthotropic media, such as fibre reinforced laminates, the assumption that the thermograph of the material corresponds to the whole laminate is governed by Eq. (5) whereas the "strain witness" hypothesis is governed by Eq. (3). As Δσ corresponds to the sum of principal stresses, in the more special case where the symmetry of the material allows it, as in the case of cross ply laminates equally reinforced in the two directions, Eq. (3) can be employed. Assumed that the material is seen by the camera as thermally isotropic, i.e., Eq. (3) is valid. As aforementioned, this assumption holds for both the "strain witness" principle [48], and materials which possess a symmetry that is seen as isotropic by the thermal camera. As soon as the material hereby is constituted by a twill weave pre-preg fabric (0°/90°), the specimen is stressed in the principal material axis.

3. Experimental

3.1. Samples preparation

CFRP repaired coupons were employed to study the interaction between critical and subcritical damage for optimum bond strength. The MTM56/CF0300 pre-preg (199 g/m²) was employed, provided by Advanced Composites Group (UK) (cure cycle: 30 min at 120 °C). The interrogated carbon fabric is a standard high strength material in twill weave format. The same material was employed for both the repair (4 layers) and the substrate (8 layers). A 5 mm circular notch was drilled (and repaired) in the middle of each substrate using a diamond drill as a typical damage scenario. Apart from a damage concept, the notch is characteristic of the methodology employed to arrest/retard the crack propagation by "stop drilling", in the case of aluminium [49] panels. Although a 5 mm notch may be small in size as a representative damage scenario in aircrafts, the strip configuration did not allow for the introduction of greater notch size. After manufacturing, samples were tabbed with 50 × 60 mm² end tabs using high shear adhesive (Epibond

1590 A/B, Huntsman), to prevent failure at the gripping area. Fig. 4 shows the examined coupon dimensions as well as the employed CFRP patch geometry.

3.2. Testing

An INSTRON 8801 universal testing machine with a maximum load capacity of ± 100 kN was employed for the coupon testing (Fig. 5a). The ultimate tensile strength of the undamaged substrate was chosen as a reference, based on the principle that the repaired structure should regain its initial strength. The ultimate tensile strength (σ_uts) of the undamaged substrate was determined by quasi static tension to be 600 ± 58 MPa according to ASTM D3039/D3039M − 08.

A total of three patched specimens were tested in 5 Hz tension-tension fatigue and stress ratio R = 0.1. Initially, fatigue testing was carried at very low stress level which was incrementally increased until debonding initiated and propagated in a stable manner. If no debonding was observed after 20,000 cycles, a 10% step increase to the next stress level was performed. More analytically, test series at 20%, 30%, 40, 50%, 60%, 65%, 70% and 80% were performed and when 80% UTS is reached, the test is run until the specimen's failure (Fig. 5b). At the last load level (80% of the σ_uts), a stable propagation of critical failure or debonding of the patch from the substrate was observed with increasing fatigue cycles, starting from the edges of the patch (critical damage). At the same stress level, considerable damage of the substrate at the edges of the drilled hole (subcritical damage) was observed. Critical failure was observed at 80% for all three coupons tested.

For the thermal response, the Jade 510-CEDIP-MIR infrared camera was employed (Fig. 5a). It features a cooled indium antimonide (InSb) detector (3–5 μm), with a frame rate ranging from 50 to 150 Hz and focal plane array (FPA) pixel format of 320 (H) × 240 (V). The thermal sensitivity of the camera is lower than 25 mK. The camera was employed in lock-in mode at a frame frequency of 50 Hz (sinusoidal frequency imposed by the loading frame was 5 Hz). The camera was positioned at approximately 1 m distance from the specimen in order to include the whole patched area in the field of view of the camera (Fig. 5a). At this distance the corresponding field of view was 208 × 156 mm² with a lateral and perpendicular resolution of 0.65 mm/pixel. The camera was through a lock-in amplifier, connected with the main controller of the servo hydraulic testing machine. The loading input of the testing machine was used as reference signal for lock-in thermographs. Therefore, synchronization of the acquisition capture frequency with the IrT image was feasible by recording the exact propagation of time between the input and output signal [50]. In all cases, the monitored surface (Fig. 5a) of the coupons was uniformly varnished black (thickness < 20 μm). The use of black matt varnish renders a uniform emissivity of the material close to that of the black

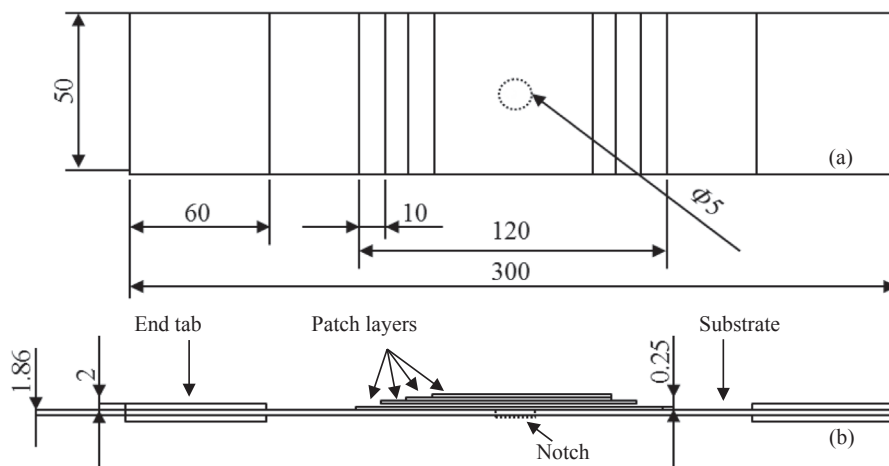Fig. 4. CFRP patch on CFRP substrate geometry; open hole at the centre of the substrate: (a) front side, (b) lateral side.
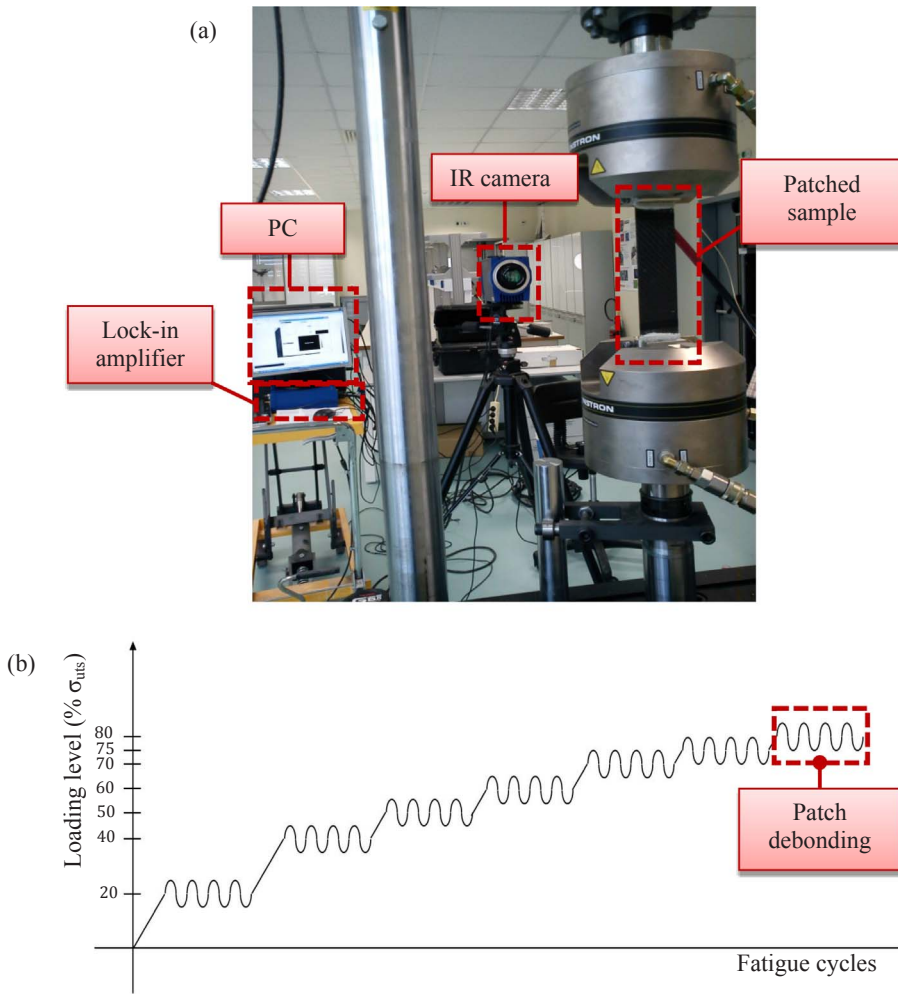
(a)

(b)

body (paint in this work ε = 0.97–1), ensures for optimum recording data and hence facilitates thermographic analysis [14,15,25,51].

4. Results and discussion

4.1. Analysis of thermographs

External or passive heating and thermal conduction with the gripping of the tested samples with the machine are assumed to be zero. The external heat supply due to radiation is considered time-dependent. Therefore, from the thermomechanical coupling formula described in [52], it is only thermoelasticity and intrinsic heat dissipation that the thermal differences on the material are attributed to. Based on the fact that the signal is linearly recorded by a thermal sensor [3] and assuming that all other parameters are constant (for small temperature changes K_m is constant), the relative stress difference induced thermoelastically, is directly related to the relative temperature difference both for the local stress difference and temperature difference σ and T, respectively and the stress σ difference and temperature T difference away from the notch σ_∞ and T_∞, respectively. Therefore, Eq. (1) can lead to:

$$\Delta\sigma \approx \Delta T = \frac{\Delta\sigma_{local}}{\Delta\sigma_\infty} = \frac{\Delta T_{local}}{\Delta T_\infty} \tag{7}$$

To prevent reader's confusion, $\Delta\sigma$ is a dimensionless parameter we use to quantitatively present the fatigue response of the component through the thermoelastic effect or the interconnection between the thermal energy vs. mechanical stresses or magnitude of stress concentration. $\Delta\sigma$ represents the relative thermal differences extracted from the thermographs that correspond to the amplitude of the recorded mechanical stress signal. After preliminary testing, the studied repaired component was found to fail as follows: the applied patch debonds from the substrate (subcritical damage) and subsequently the structure fails at the locus of the circular notch (critical failure). Therefore, the stress analysis is concentrated in the vicinity around the notched area. The stress amplitude of the thermoelastic signal is employed as a parameter for monitoring fatigue damage through the thermomechanical coupling. The hysterestic heat source has been found to be two orders of magnitude lower than the thermoelastic energy source. In this respect and since any hysterestic behaviour is taking place only prior to failure, it is not taken into account in the analysis of developed stresses during fatigue.

In other words, the recorded normalised thermal (stress amplitude) gradient on the specimen surface is equal (proportional) to the normalised stress gradient. In this way, all amplitude images may be transformed to stress maps ($\Delta\sigma$) simply by normalising the local stress amplitude values by the stress amplitude value away from the induced stress concentration, or the far field amplitude value (Eq. (7)).

Fig. 6a shows the interrogated axis on the repaired coupon. In Fig. 6b, the typical stress concentration vs. position graph at the vicinity of the notch is analysed for the employed material configuration. The solid grey line (Fig. 6b) depicts the composite $\Delta\sigma$ vs. distance graph. This comprises the stress pattern that is due to the presence of the notch (dashed line) and the local stress variation that are due to the twill weave pattern (carbon fabric) of the interrogated material (solid black line). It should be argued at this point, the stress variations due to the
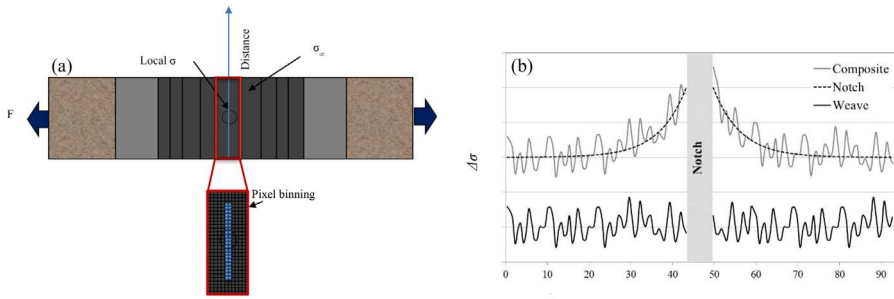
Fig. 6. $\Delta\sigma_{local}/\Delta\sigma_{\infty}$ ($=\Delta\sigma$) vs. distance: (a) location of measurements, (b) components of the composite graph: weaving pattern and notch induced $\Delta\sigma$.
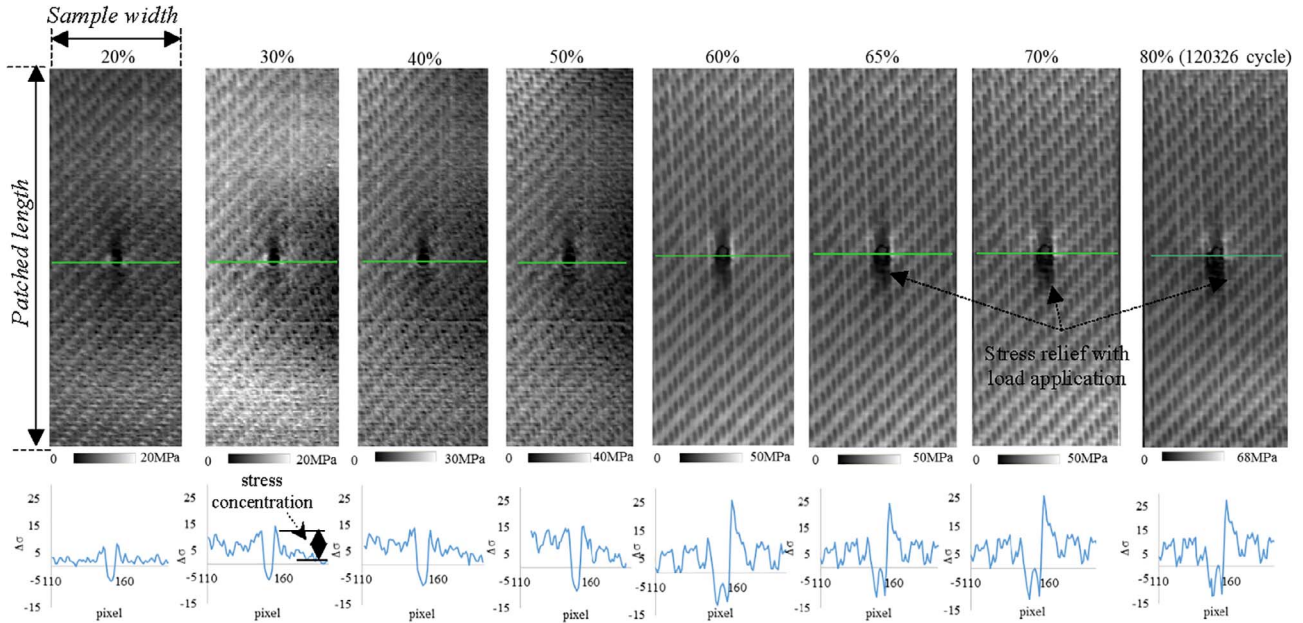

Fig. 7. Progress of delamination/separation/detachment of patch from the substrate during fatigue loading from 20 to 80% of σ_{uts}; respective normalised amplitude versus distance (pixels) graphs.
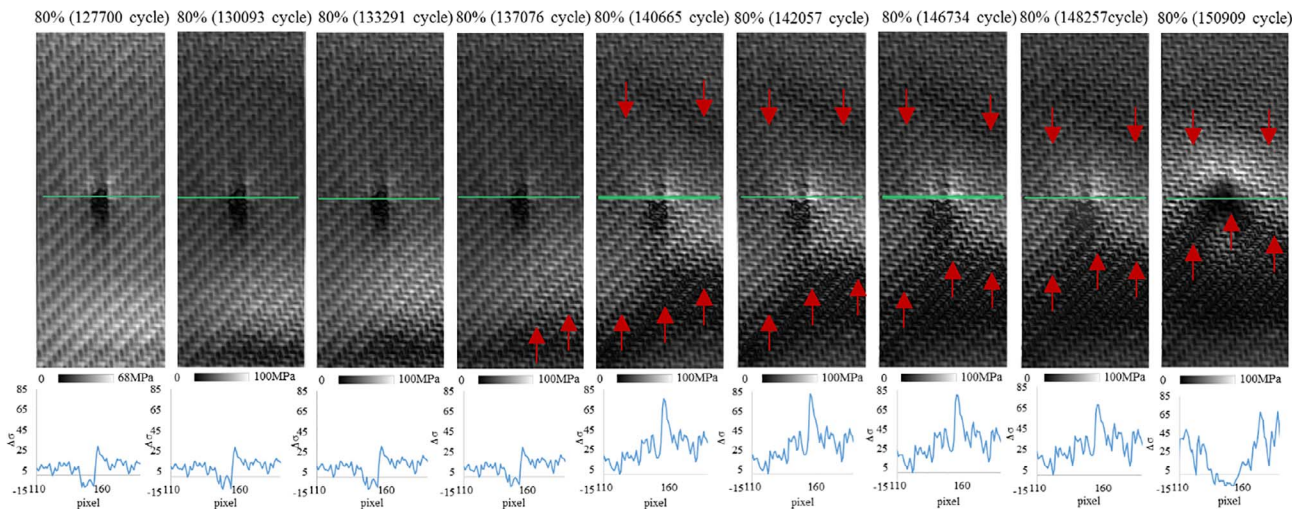

Fig. 8. Progress of delamination/separation/detachment of patch from the substrate during fatigue loading at 80% of σ_{uts} from cycle 127,700 cycle until rupture; respective normalised amplitude versus distance (pixels) graphs.

weaving pattern were consistently present in all thermographs. As they remained constant throughout the conducted experiments unless critical or subcritical damage altered the amplitude variation at the specific area, they are positively attributed to stress variations inherent of the interrogated system, and not noise. In this respect, the stress fields from both the notch (dashed line) and the weaving pattern (solid black line) are superimposed to result to the stress concentration depicted as the composite $\Delta\sigma$ (solid grey line). For the case under study, in order to calculate the $\Delta\sigma$ due to the presence of the notch, all local stress amplitude values (extracted by the thermographs shown in Figs. 7 and 8) were normalised by the mean stress amplitude value from the weaving pattern away from the notch σ_{∞} (Fig. 6a). As is obvious, the locally

induced stress by the weaving pattern is cumulatively contributing to the stress pattern and the induced damage either constructively or destructively. As the "weave induced" stresses are superimposed to the "notch induced" stresses, they increase the possibility of local failure where the stress intensity factor is maximum. As a result, the following analysis will be based on cumulative stress development and not only on the "notch induced" stress concentration.

Fig. 7 represents amplitude snapshots at 20%, 30%, 40%, 50%, 60%, 65%, 70% and (early) 80% load levels, as recorded by the thermal camera. For 20%, 30%, 40%, 50%, 60%, 65% and 70% load levels, images were extracted towards the end of each test level i.e. at the steady state. With respect to 80% load level, images were more frequently extracted in order to showcase the more significant (visible) transition phases taking place (Fig. 8). Up until the early (120,326 cycle) fatigue cycles at 80%, the amplitude images did not change for all three tested coupons. On the contrary, in the case of 80% load level (Fig. 8), the amplitude image started changing characteristically during the fatigue loading until coupon failure. The deterioration trace of the patch/substrate interface (Fig. 8) is highlighted by arrows on some of the images. In all stress levels, stress concentration areas are depicted as bright spots in the corresponding snapshots around the circular notch or as bright areas at the edges of the patch, particularly at the loading (bottom) side of the test frame.

More specifically, the 1st thermal image in Fig. 7 is typical of the stress state at 20%, as no notable changes were recorded throughout the loading process. Stress concentrations can clearly be seen as bright spots on either side of the notch, where stresses are expected to be maximum. The application of higher stress levels did not alter the stress distribution on the sample surface which also remained stable for approximately 20 k cycles throughout the loading process until 60% σ$_{uts}$. A slight increase in stresses was then recorded which altered the thermographic images in the critical area around the notch which remained practically constant for another 40 k loading cycles. In the case of 80% load level (Fig. 8), the amplitude images did not alter for approximately more 20 k cycles. As can be seen, the amplitude disturbance at the vicinity of the notch clearly covered more extended area, with less prominent bright spots and characteristic dark areas which corresponded to unloaded (or less loaded) areas of the coupon. The examination of these thermographs led to the conclusion that stress concentrations caused initiation and propagation of stress-relief damage mechanisms, characteristic of the damage tolerant behaviour of the composite laminates: longitudinal splitting could be clearly seen on either side of the notch. This splitting occurred on the side of the specimen where the test frame applies the loading (bottom area in the thermograph). The same trend was observed in the thermal image cycle 120,326 of 80% loading (Fig. 7), where bright areas are less prominent at the edges of the notch and the damage manifested by the dark areas is slightly increased. Amplitude changes became more visible after approximately 140 k cycles. Stress concentrated areas mostly from the bottom part for the notch (loading side), started pronouncedly approaching the notch reflecting the gradual detachment of the patch from the substrate. Complete detachment of the patch (critical damage) occurred at approximately 160 k loading cycles which exposed the circular notch and led to the immediate failure of the component due to subcritical damage.

In both Figs. 7 and 8 the measured corresponding stress amplitude along the line drawn on the thermal images is plotted against the image pixels, normalised by the mean stress amplitude value away from the notch (Eq. (7), Fig. 6a). This amplitude corresponds to the emitted energy received by the camera, and is directly proportional to the recorded temperature on the specimen surface. Note that the loading cycles shown next to the amplitude images (Figs. 7 and 8) refer to the total number of cycles of loading since the onset of the step-wise fatigue testing at 20% of σ$_{uts}$.

In this way, the corresponding relative Δσ at each stress level could be estimated and plotted as a function of the stress level or the fatigue loading cycles (Fig. 9). Graphs in Fig. 7 depict the transition from 20%
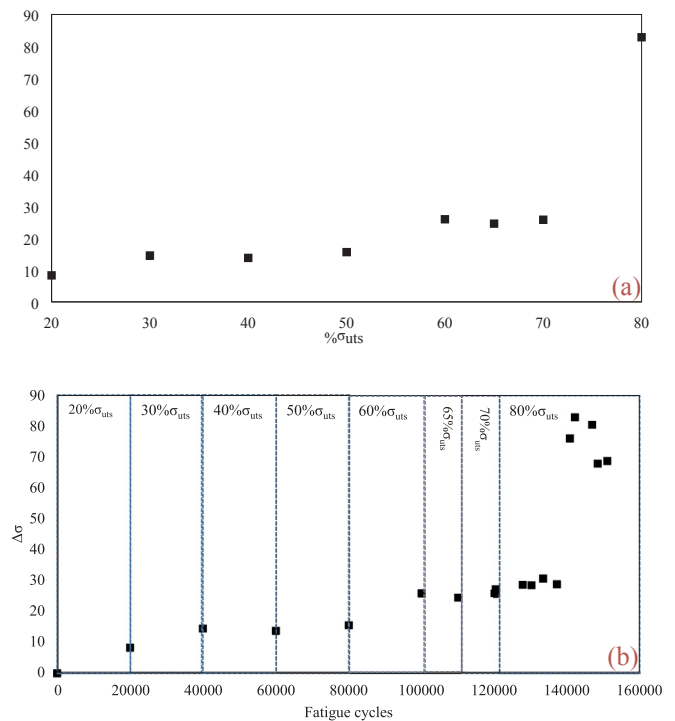

Fig. 9. Stress concentration vs. fatigue cycles from 20% to 80% of the σ$_{uts}$ and until rupture.

to early 80% which leads to the increase of cumulative stresses on the right side of the notch seen as bright spot. It is interesting to note that the stress concentration pattern in Fig. 7, remains almost stable until the 60% σ$_{uts}$, a fact that strongly indicates that the recorded stress variation is real and cumulative due to the notch and the weaving pattern. After that, Δσ exhibits a slight increase which oscillates around a constant value for 40 k cycles more (100–140 k cycles). In Fig. 8 the propagation of critical damage is manifested in the thermal images as areas of stress relief on the surface of the repaired composite coupon, or bright areas that propagate towards the centre of the coupon with further cyclic loading. The critical debonding process was also monitored in a previous work for unnotched patched aluminium coupons [14]. The non-monotonic behaviour of the amplitude peaks (stress concentration) can be explained by two competing mechanisms: (i) the gradual loss of lateral support due to the critical debonding results to the increase in the Δσ which reaches a mean value of ~25, while at this stage (ii) extensive longitudinal splitting (manifested as dark ribbons underneath the notch area) leads to the relief of the stress concentration. At the same time, the propagating critical failure gradually reaches the notch area (Fig. 8, cycle 148,257) which results in the catastrophic transverse failure of the coupon after a total of approximately 160 k cycles.

In Fig. 8, the bright areas on the top and bottom (mostly) of the image (patch edges) were clearly confined towards the middle of the specimen, denoting the onset and propagation of debonding. At the same time, the bright areas around the circular notch became more pronounced, as the localized stresses became gradually less inhibited by the failing patch. Further cyclic loading induced asymmetric debonding of the patch which significantly altered the stress distribution on the surface. Catastrophic failure took place at 150,909 cycles when the debonding front merged with the notch-induced stress concentration.

4.2. Analysis of thermographic data

Fig. 9 shows the maximum Δσ (peak values of Δσ vs. distance plots from Figs. 7 to 8) as a function of the stress level and the total loading
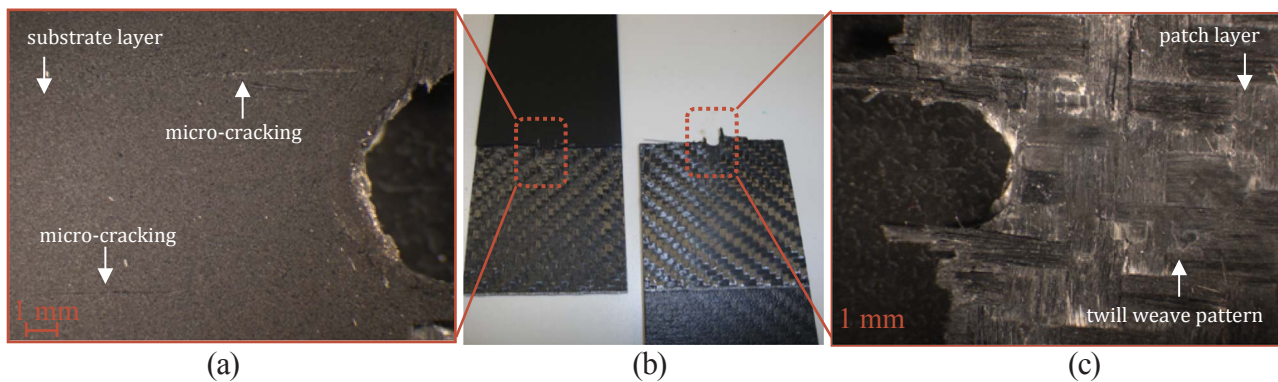
Fig. 10. (a, c) Post failure stereoscopic images of the patched specimen, (b) post failure image.

cycles (number of cycles since the onset of the step-wise cyclic loading) until final failure at approximately total ~160 k cycles. In the specific geometry, the resolution of the amplitude picture was 0.65 mm/pixel. In Fig. 9, the plotted curve corresponds to the binning of two pixel values (Fig. 6a) at the centre of the notch, i.e. a resolution of 1.3 mm for a 5 mm notch. This was performed so that the centre of the notch was always included in the measurements. Binning decreases the uncertainty in the amplitude measurements due to the inherent resolution limitations, but it may provide a slight underestimation of the measured amplitude/stress concentration values. However, this limitation does not affect the observations regarding the evolution of the stress concentration values. There is an expected gradual increase in $\Delta\sigma$ with stress levels which is due to the increase in applied stress. This stress concentration increase also observed as bright spots at the two sides of the notch, led to longitudinal splitting shown as dark areas in the amplitude images (Fig. 7), which is obviously a local relief of the stress concentrations. Changes in $\Delta\sigma$ are within the recorded variation in the system up until 60% of σ_{uts}. In this respect, the $\Delta\sigma$ remains relatively constant at an approximate value of 15 ($\Delta\sigma$). In addition, the thermographs remained relatively unaltered during the fatigue loading suggesting that the damage induced heat is not significant compared to the thermoelastically induced temperature variations, i.e. if hysteretic phenomena were dominant, the local temperature increase would mask the increase in the stress concentration.

As observed for all tested coupons, the patch gradually debonded and the specimen failed catastrophically by a transverse crack at the vicinity of the notch. It is interesting to note that for approximately 80 k cycles there is little or no change in the $\Delta\sigma$ which oscillates around a value of 15 (stage I fatigue – Fig. 2). Thereafter, there is a slight increase to a value of 25. Interestingly enough, $\Delta\sigma$ remains stable again around a value of 25–30 (stage II fatigue – Fig. 2). The constant loading frame follows a substantial increase that reaches a maximum of approximately 80 (stage III fatigue – Fig. 2) which falls back to ~67 at the time of the failure of the coupon at approximately 160 k cycles. A closer examination of the amplitude images may justify the non-monotonic behaviour of the $\Delta\sigma$ and the subsequent damage profile with cyclic loading which follows a characteristic fatigue degradation trend (Fig. 2). As was initially postulated, thermoelastic phenomena do not affect the mean temperature or the relative amplitude values of the system which correspond directly to stress concentration. However, every recorded increase in amplitude values, which here is argued as stress concentration, corresponds to damage incidents. More specifically, at approximately 146,000 loading cycles (Fig. 9), a significant crack incident led to abrupt elevation of the stress amplitude values and the subsequent modification of the thermoelastic behaviour. This is a characteristic hysteretic phenomenon which surpasses the elastic at that point and prevails until the final fracture of the component. Stress concentration values decay when internal stresses reach a maximum ($\Delta\sigma = 80$ – Fig. 9) for the given material. As a result, stresses are

relieved together with the rupture of the coupon. Similar observation presented in Fig. 9 was reported by R. Steinberger et al. [53]. This is characteristic of a hysteretic energy dissipation effect due to intrinsic damage phenomena. Beyond the fatigue limit internal damage leads to significant temperature increase and subsequent heat dissipation which can be detected by the thermal camera [41]. It could be assumed that the 80% σ_{uts} corresponds to the fatigue limit of the studied repaired component.

End of testing was followed by coupon separation in two parts. Both parts were examined using an optical microscope. Post failure pictures of the coupon exhibiting the brittle failure exactly at its centre are shown in Fig. 10. The magnification of the area of the notch (substrate part) (Fig. 10b), revealed the existence of cracks parallel to the loading axis which decreased the stress concentration with the incremental increase of the load level (Fig. 10a). The optical examination of the failed coupon also revealed the longitudinal cracks (Fig. 10a) which led to the relief in the stress concentration captured in Fig. 7. Fig. 10c is a magnification of the detached part which reveals the twill weave pattern of the employed pre-preg carbon fabric.

5. Conclusions

The main objective of the present paper was to investigate the dynamic response of bonded patch repaired components using lock-in thermography. Thermomechanical coupling was employed to study thermoelastic (reversible) and hysteretic (irreversible) phenomena that allow to quantify the critical and subcritical damage due to cyclic mechanical loading.

CFRP substrates with a circular notch were repaired using tapered CFRP patches. The relative stress amplitude variations at the vicinity of the notch were found to correspond to local stress variations or stress maps. In other words, the relative stress amplitudes as recorded by the thermal camera are equivalent to the stresses at the locus of any present discontinuity. These were identified and quantified by simply normalising the amplitude profile at the vicinity of the notch to the recorded amplitude away from the notch along a transverse straight line that dichotomised the crack.

The fatigue loading of the specimens at low stress levels showed that the magnitude of local stresses at the notch remained practically constant. At relatively higher fatigue level, significant debonding initiated and propagated. The debonding process along with the evolution of the stresses at the vicinity of the notch were clearly identified and recorded. This non monotonic behaviour followed a characteristic fatigue degradation trend which is attributed to the critical debonding failure of the patch in combination with the damage tolerant behaviour of the tested component.

Summarizing, LT can evidently provide qualitative and quantitative information in relation to the repair efficiency before the qualification of any bonded patch for aircraft application.

References

[1] Hull D, Clyne TW. An introduction to composite materials. Cambridge University Press; 1996.

[2] Rose AABRJF. Advances in the bonded composite repair of metallic aircraft structure. Elsevier; 2002. p. 530.

[3] Stanley P, Chan WK. Quantitative stress analysis by means of the thermoelastic effect. J Strain Anal Eng Des 1985;20:129–37.

[4] Meola C, Carlomagno GM, Squillace A, Vitiello A. Non-destructive evaluation of aerospace materials with lock-in thermography. Eng Fail Anal 2006;13:380–8.

[5] Meola C, Carlomagno GM. Recent advances in the use of infrared thermography. Meas Sci Technol 2004;15:R27–58.

[6] Grammatikos S, Kordatos E, Barkoula NM, Matikas T, Paipetis A. Repair integrity monitoring of composite aerostructures using thermographic imaging. 2010.

[7] Kordatos EZ, Myriounis DP, Hasan ST, Matikas TE. Monitoring the fracture behavior of SiCp/Al alloy composites using infrared lock-in thermography. 2009.

[8] Grammatikos SA, Kordatos EZ, Aggelis DG, Matikas TE, Paipetis AS. Critical and subcritical damage monitoring of bonded composite repairs using innovative non-destructive techniques. 2012. p. 834611-9.

[9] Myriounis DP, Kordatos EZ, Hasan ST, Matikas TE. Crack-tip stress field and fatigue crack growth monitoring using infrared lock-in thermography in a359/sicp composites. Strain 2011;47:e619–27.

[10] Kordatos EZ, Aggelis DG, Matikas TE. Monitoring mechanical damage in structural materials using complimentary NDE techniques based on thermography and acoustic emission. Composites Part B.

[11] Bremond P. New developments in thermoelastic stress analysis by infrared thermography. 2007.

[12] Krstulovic-Opara L, Klarin B, Neves P, Domazet Z. Thermal imaging and thermoelastic stress analysis of impact damage of composite materials. Eng Fail Anal 2011;18:713–9.

[13] Thomson W. On the dynamical theory of heat. Trans R Soc Edinburgh 1853;20:261–83.

[14] Grammatikos SA, Kordatos EZ, Barkoula NM, Matikas TE, Paipetis AS. Innovative non-destructive evaluation and damage characterisation of composite aerostructures using thermography. Plast, Rubber Compos 2011;40:342–8.

[15] Grammatikos SA, Kordatos EZ, Matikas TE, Paipetis AS. Real-time debonding monitoring of composite repaired materials via electrical, acoustic, and thermographic methods. J Mater Eng Perform 2014;23:169–80.

[16] Kordatos EZ, Dassios KG, Aggelis DG, Matikas TE. Rapid evaluation of the fatigue limit in composites using infrared lock-in thermography and acoustic emission. Mech Res Commun 2013;54:14–20.

[17] Thomson W. II. On the dynamical theory of heat, with numerical results deduced from Mr. Joule's equivalent of a thermal unit, and M. Regnault's observations on steam. Philos Mag Ser 4 1852;4:8–21.

[18] Ummenhofer T, Medgenberg J. On the use of infrared thermography for the analysis of fatigue damage processes in welded joints. Int J Fatigue 2009;31:130–7.

[19] Quinn S, Dulieu-Barton JM, Eaton-Evans J, Fruehmann RK, Tatum PJ. Thermoelastic assessment of plastic deformation. J Strain Anal Eng Des 2008;43:451–68.

[20] Belakhdar K, Tounsi A, Benyoucef S, Bedia EAA, El Hassar SM. On the reduction of the interfacial stresses in a repaired beam with an adhesively bonded FRP plate. Compos Interfaces 2010;17:1–14.

[21] Baker AA. Repair of cracked or defective metallic aircraft components with advanced fibre composites—an overview of Australian work. Compos Struct 1984;2:153–81.

[22] Dulieu-Barton JM, Stanley P. Development and applications of thermoelastic stress analysis. J Strain Anal Eng Des 1998;33:93–104.

[23] Pitarresi G, Patterson EA. A review of the general theory of thermoelastic stress analysis. J Strain Anal Eng Des 2003;38:405–17.

[24] Kordatos EZ, Aggelis DG, Matikas TE. Monitoring mechanical damage in structural materials using complimentary NDE techniques based on thermography and acoustic emission. Composites Part B 2012;43:2676–86.

[25] Pavlopoulou S, Grammatikos SA, Kordatos EZ, Worden K, Paipetis AS, Matikas TE, et al. Continuous debonding monitoring of a patch repaired helicopter stabilizer: damage assessment and analysis. Compos Struct 2015;127:231–44.

[26] Stanley P, Dulieu JM. Accuracy and precision in the thermoelastic stress analysis technique. In: Hyde TH, Ollerton E, editors. Applied stress analysis. Netherlands: Springer; 1990. p. 627–38.

[27] Mountain DS, Webber JMB. Stress pattern analysis by thermal emission (SPATE). 1979. p. 189–96.

[28] Reifsnider KL, Williams RS. Determination of fatigue-related heat emission in composite materials. Exp Mech 1974;14:479–85.

[29] Charles JA, Appl FJ, Francis JE. Using the scanning infrared camera in experimental fatigue studies. Exp Mech 1975;15:133–8.

[30] Stanley P, Chan WK. The application of thermoelastic stress analysis techniques to composite materials. J Strain Anal Eng Des 1988;23:137–43.

[31] Bakis CE, Reifsnider KL. The adiabatic thermoelastic effect in laminated fiber composites. J Compos Mater 1991;25:809–30.

[32] Wong AK. A non-adiabatic thermoelastic theory for composite laminates. J Phys Chem Solids 1991;52:483–94.

[33] Cunningham PR, Dulieu-Barton JM, Dutton AG, Shenoi RA. The effect of ply lay-up upon the thermoelastic response of laminated composites. 2002. p. 325–36.

[34] El-Hajjar R, Haj-Ali R. A quantitative thermoelastic stress analysis method for pultruded composites. Compos Sci Technol 2003;63:967–78.

[35] Haj-Ali R, Elhajjar R. An infrared thermoelastic stress analysis investigation of single lap shear joints in continuous and woven carbon/fiber epoxy composites. Int J Adhes Adhes 2014;48:210–6.

[36] Pitarresi G, Found MS, Patterson EA. An investigation of the influence of macroscopic heterogeneity on the thermoelastic response of fibre reinforced plastics. Compos Sci Technol 2005;65:269–80.

[37] Dulieu B, Fulton, Stanley. The analysis of thermoelastic isopachic data from crack tip stress fields. Fatigue Fract Eng Mater Struct 2000;23:301–14.

[38] Montesano J, Fawaz Z, Bougherara H. Use of infrared thermography to investigate the fatigue behavior of a carbon fiber reinforced polymer composite. Compos Struct 2013;97:76–83.

[39] Melvin AD, Lucia AC, Solomos GP. The thermal response to deformation to fracture of a carbon/epoxy composite laminate. Compos Sci Technol 1993;46:345–51.

[40] Talreja R. Fatigue of composite materials: damage mechanisms and fatigue-life diagrams. Proc R Soc London, Ser A 1981;378:461–75.

[41] De Finis R, Palumbo D, Ancona F, Galietti U. Fatigue limit evaluation of various martensitic stainless steels with new robust thermographic data analysis. Int J Fatigue 2015;74:88–96.

[42] Kulkarni R, Ochoa O. Transverse and longitudinal CTE measurements of carbon fibers and their impact on interfacial residual stresses in composites. J Compos Mater 2006;40:733–54.

[43] Rogers K, Kingston-Lee D, Phillips L, Yates B, Chandra M, Parker S. The thermal expansion of carbon-fibre reinforced plastics. J Mater Sci 1981;16:2803–18.

[44] Grammatikos SA, Kordatos EZ, Matikas TE, David C, Paipetis AS. Current injection phase thermography for low-velocity impact damage identification in composite laminates. Mater Des 2014;55:429–41.

[45] Fruehmann RK, Dulieu-Barton JM, Quinn S. Thermoelastic stress and damage analysis using transient loading. Exp Mech 2010;50:1075–86.

[46] Wong AK, Jones R, Sparrow JG. Thermoelastic constant or thermoelastic parameter? J Phys Chem Solids 1987;48:749–53.

[47] Dunn SA, Lombardo D, Sparrow JG. The mean stress effect in metallic alloys and composites. 1989. p. 129–42.

[48] Pitarresi G, Galietti U. A quantitative analysis of the thermoelastic effect in CFRP composite materials. Strain 2010;46:446–59.

[49] Aglan H, Rowell T, Ahmed T, Thomas R. Durability assessment of composite repairs bonded to aircraft structures. J Adhes Sci Technol 1999;13:127–48.

[50] Maldague X. Applications of Infrared Thermography in NonDestructive Evaluation. In: Testing TiON (ed.) Pramod Rastogi e-Journal of Nondestructive Testing & Ultrasonics; 2000. p. 591–609.

[51] McKelvie J. Consideration of the surface temperature response to cyclic thermoelastic heat generation. 1987. p. 44–55.

[52] Luong MP. Fatigue limit evaluation of metals using an infrared thermographic technique. Mech Mater 1998;28:155–63.

[53] Steinberger R, Valadas Leitão TI, Ladstätter E, Pinter G, Billinger W, Lang RW. Infrared thermographic techniques for non-destructive damage characterization of carbon fibre reinforced polymers during tensile fatigue testing. Int J Fatigue 2006;28:1340–7.